


Article

A Flood Risk Management Program of Wadi Baysh Dam on the Downstream Area: An Integration of Hydrologic and Hydraulic Models, Jizan Region, KSA

Mazen M. Abu-Abdullah ¹, Ahmed M. Youssef ^{1,2,*} , Norbert H. Maerz ³, Emad Abu-AlFadail ¹, Hasan M. Al-Harbi ¹ and Nasser S. Al-Saadi ¹

¹ Geological Hazards Department, Applied Geology Sector, Saudi Geological Survey, P.O. Box 54141, Jeddah 21514, Kingdom of Saudi Arabia; abuabdullah.mm@sgs.org.sa (M.M.A.); abualfadhael.ey@sgs.org.sa (E.A.); harbi.hm@sgs.org.sa (H.M.A.); saadi.ns@sgs.org.sa (N.S.A.)

² Geology Department, Faculty of Science, Sohag University, Sohag 82524, Egypt

³ Director of the Rock Mechanics and Explosives Research Center, Missouri University of Science and Technology, Rolla, MO 65409, USA; norbert@mst.edu

* Correspondence: amyoussef70@gmail.com;

Received: 2 December 2019; Accepted: 30 January 2020; Published: 3 February 2020



Abstract: For public safety, especially for people who dwell in the valley that is located downstream of a dam site, as well as the protection of economic and environmental resources, risk management programs are urgently required all over the world. Despite the high safety standards of dams because of improved engineering and excellent construction in recent times, a zero-risk guarantee is not possible, and accidents can happen, triggered by natural hazards, human actions, or just because the dam is aging. In addition to that is the impact of potential climate change, which may not have been taken into account in the original design. A flood risk management program, which is essential for protecting downstream dam areas, is required. Part of this program is to prepare an inundation map to simulate the impact of dam failure on the downstream areas. The Baysh dam has crucial importance both to protect the downstream areas against flooding, to provide drinking water to cities in the surrounding areas, and to use the excess water for irrigation of the agricultural areas located downstream of the dam. Recently, the Kingdom of Saudi Arabia (KSA) was affected by extraordinary rainstorm events causing many problems in many different areas. One of these events happened along the basin of the Baysh dam, which raised the alarm to the decision makers and to the public to take suitable action before dam failure occurs. The current study deals with a flood risk analysis of Wadi Baysh using an integration of hydrologic and hydraulic models. A detailed field investigation of the dam site and the downstream areas down to the Red Sea coast has been undertaken. Three scenarios were applied to check the dam and the reservoir functionality; the first scenario at 100- and 200-year return period rainfall events, the second scenario according to the Probable Maximum Precipitation (PMP), and the third scenario if the dam fails. Our findings indicated that the Baysh dam and reservoir at 100- and 200-year rainfall events are adequate, however, at the PMP the water will spill out from the spillway at $\sim 8900 \text{ m}^3/\text{s}$ causing flooding to the downstream areas; thus, a well-designed channel along the downstream wadi portion up to the Red Sea coast is required. However, at dam failure, the inundation model indicated that a vast area of the section downstream of the dam will be utterly devastated, causing a significant loss of lives and destruction of urban areas and agricultural lands. Eventually, an effective warning system and flood hazard management system are imperative.

Keywords: dam failure; inundation; flood hazard; management; Baysh; KSA

1. Introduction

Flood hazards are considered one of the most significant natural hazards that cause damage, destruction, and loss of human property as well as injuries and death [1–7]. These floods can halt all further development activities and efforts and cause countries' resources to be exhausted in the mitigation of the adverse impacts of these flood hazards. Flash floods in arid areas are generally related to an extraordinary increase in the precipitation values resulting in high discharge at the downstream basin portions [8]. Due to scarcity of rainfall in the arid regions, there is a rapid increase in the uncontrolled urban sprawl along the wadis passes and their floodplain areas; areas which will be under a significant risk due to flash floods [1–3,9–11]. The flash flood impacts have increased in many areas all over the world especially with recent climate changes [12–16]. Various causative factors are contributors to flash floods (e.g., hydrological and meteorological characteristics, soil and land-use types, geological structures, geomorphology, and vegetation) [8,17,18].

Recently, heavy rainfall events have triggered flash floods in various areas in the Middle East countries. In Morocco, three flash flood events in 1995, 2002, and 2008 left 268 dead [19]. In Algeria, flash floods and mudslides in 2001 caused more than 700 to perish and thousands to be left homeless [20]. In Chad, 2012, floods displaced hundreds of thousands and swamped 255,720 ha of croplands [21]. In Egypt, flash floods frequently occur in many areas, e.g., in 2016, 22 people were killed in the Ras Gharib area [22]. In the Kingdom of Saudi Arabia (KSA) flash floods have occurred in many areas (e.g., Jeddah City in the years 2009, 2011, 2015, 2017, and 2018; Al-Lith in 2018, and Al Riyadh in 2015 and 2018). The city of Jeddah was hit by the most severe events in 2009 and 2011 causing a death toll of 113 people, damage to more than 10,000 homes, and the destruction of 17,000 vehicles [23,24].

Many flood events are related to dam failures [25]. Dams, around the world, have been established for various purposes (e.g., flood prevention, electricity generation, agriculture activities, and water supply [26]. Unfortunately, many of these dams have failed due to many reasons (e.g., structural problems, earthquakes, landslides, foundation failure, unprecedented extreme rainfalls, and high-water flows [27,28]. Most of the dam failures are triggered by flooding due to inadequate capacity of the reservoir and spillway and the consequent overtopping of water over the dam crest. The Kaddam dam in India failed due to overtopping in 1958 [29]. The Banqiao dam and the Shimantan dam in China collapsed due to the overtopping in 1975, causing the death of 85,000 people [25]. In the KSA, dam construction activities began around two decades ago. However, in recent years many dam areas were affected by extraordinary rainfall events. These rainfall events are increasing the threat to communities and putting significant stresses on governments. Many dam failures have happened in some areas in the KSA causing inundation problems. Fortunately, these dams were small ones (e.g., the Um Al-Khair dam in Jeddah, failed in 2011) [23,24] and the Al-Lith dam failed after severe rainfall in November 2018)).

However, to protect the downstream areas of any dam, the development of an emergency action plan is required. This needs an accurate estimation of the inundation level and extent at the downstream areas of the dam site [30]. Flood prevention measures, in many areas, are required to decrease and minimize the enormous, potentially devastating impact to urban and agricultural areas and infrastructure units (roads, highways, bridges, pipelines and electricity lines, and railways) [31]. Effective early warning systems and emergency plans for flooding episodes are required in many arid countries [32,33]. These systems will provide the authorities, governments, and policymakers the ability to mitigate or prevent potential damage due to floods. Liu and De Smedt [34] mentioned that understanding the mitigative techniques of flooding requires new insights in hydrological research by using geographic information system (GIS), digital soil-type maps, topography, and land use/land cover data. Generally, the assessment of flood damage relies on the interaction between flood levels and human activities. Changes in modern society, due to population increase, economic development, uncontrol urbanization, and deforestation make society more vulnerable to flooding [17,35]. The scale and impact of flood crises on societies (people, property, industry, and economics) will increase if there is no application of effective flood risk management [36]. Recently, many effective methods

have been introduced in flood risk management, including hydrodynamic models and flood inundation mapping [37–43].

The fundamental objectives of the current study are to evaluate the different hydrological and hydraulic responses of the Wadi Baysh dam at 100-year and 200-year return period rainfall events and at Probable Maximum Precipitation (PMP) under different scenarios for the dam reservoir. In addition, the goal is to evaluate the conditions of the dam downstream at the time of dam failure due to water overtopping. Various variables control flood intensity and frequency, such as rainfall characteristics, drainage networks, basin conditions, and land use/land cover distributions. In the case where a dam is currently present, the dam properties will be used. To achieve these objectives in this research, an integrated approach using different models was used. A Watershed Modelling System (WMS) was used to extract the drainage networks and drainage basins characteristics. The Hydrologic Engineering Center-Hydrologic Modeling System (HEC-HMS) was used to simulate the rainfall-runoff processes of the basins. The Soil Conservation Service (SCS) model was used to evaluate the rainfall-runoff of the catchments. The Simplified Dam Break (SMPDBK) model of WMS was applied to assess the dam failure (dam break), where three substantial elements are required including the estimation of the outflow hydrograph of the dam break, hydrographs of the routing methodology of the waters released by dam breaks through the downstream wadis, and the determination of the inundation levels along the downstream areas. These studies were carried out with the help of Geographic Information Systems (GIS) that are used to prepare the Digital Elevation Models (DEMs) and for analysis of remote sensing images, geologic maps, soil types, and land-use/land-cover data. A field investigation was applied to validate and verify the inundation model. This study is crucial work in the KSA for flash flood assessment and to manage future flood risks due to dam failure.

2. Study Area Characteristics and Problem Statement

2.1. Location and Geology

The Wadi Baysh basin is located in the Jazan region, in the southwestern portion of the Kingdom of Saudi Arabia (Figure 1a). It is bounded by longitudes between 42°20'30" and 43°27'54" E and latitudes between 17°02'57" and 18°04'12" N. There are many urban areas distributed along the downstream portion of the dam site (Figure 1b,c). Prior to the dam construction, the downstream area was vulnerable to flash floods from Wadi Baysh. This wadi drains the high mountain areas that are located upstream of the dam site into the floodplain area located downstream of the dam site, before entering the Red Sea. The upstream catchment of the dam site is characterized by many tributaries (e.g., Wadi Dafa, Wadi Dhibah, Wadi Lajb, Wadi Bishah, and Wadi Yakhraf). The elevation of the study area ranges between 0 m above mean sea level (on the Red Sea coast) and 2750 m (at the eastern portion of the basin).

Interpretation of the geological maps (quadrangles GM-77C and GM-75C) (1:250,000-scale) acquired from the Saudi Geological Survey database for the study area revealed the rock succession in the Wadi Baysh area and is shown in Figure 1b. The succession is composed of PreCambrian basement rocks (mainly intrusive and volcanic rocks with lesser amounts of metamorphic rocks), which compose the main constituent of the upstream basin of the dam site. Sedimentary rocks (sandstone and calcareous rocks) overlay the PreCambrian rocks and are concentrated in the area surrounding the dam site and at the middle area of the upstream basin. The sedimentary rocks are overlaid with loose and/or consolidated Quaternary deposits (alluvial and terrace deposits) and cover a large portion of the downstream area of the dam site. Sabkha deposits are located along the mouth of the wadi along the Red Sea coast. Finally, sand dunes are found in the downstream basins of the dam site. There are many urban, agricultural, and reclamation areas distributed along the downstream portion of the dam site (on the wadi course and its floodplain sediments). The study area is distinguished by great variability of temperature resulting in a very hot summer and mild winter. According to climate classification, the study area belongs to the hot dry desert (BWh) climate zone [44,45].

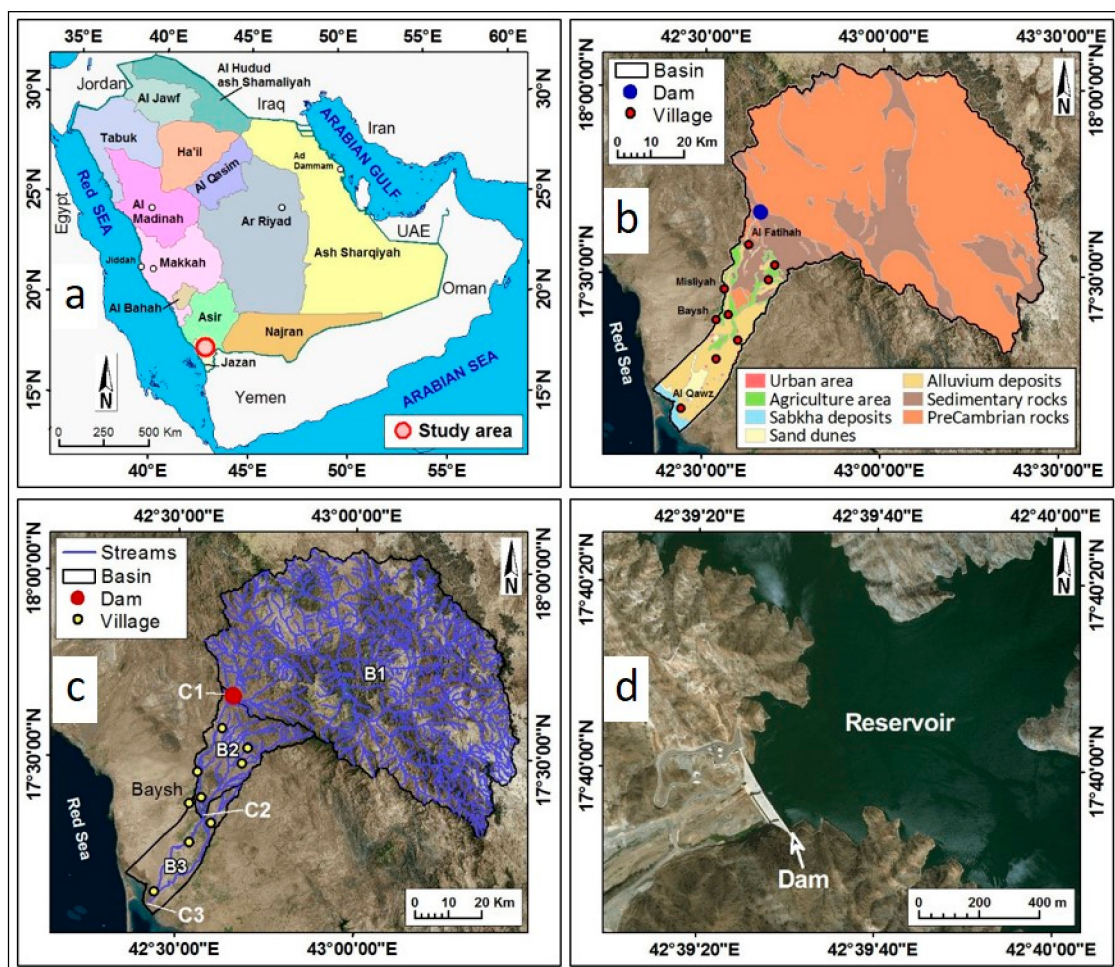


Figure 1. Showing: (a) study area location in the KSA map; (b) a combination of land use/land cover and soil maps of the Wadi Baysh catchment area; (c) drainage networks and sub-catchments of Wadi Baysh (B1, B2, and B3); (d) dam location and a portion of the dam's reservoir. Note that the location of villages (urban areas) along the downstream of the dam site are shown in Figure 1b,c, and the critical sites are shown as C1, C2, and C3 in Figure 1c.

2.2. Dam and Reservoir Characteristics

The Baysh dam was constructed in 2009 along the main stream of Wadi Baysh. It located at Longitude 42°39'28" E, and Latitude 17°39'57" N (Figure 1d). According to the data obtained from the Ministry of Environment, Water, and Agriculture, confirmed through field visits to the dam site and its surroundings, it was found that the dam was constructed to control the flood water that collected from the upstream drainage basin (with an area of ~4745 km²). It also provides water to some cities. It is a solid gravity dam, ~340 m long and ~74 m high. The spillway level is ~62 m high and ~112 m wide (consisting of eight openings with ~14 m width for each). The top barrier of the dam is 1.51 m high, the spillway depth is ~10.49 m, and the footprint of the reservoir at the level of the spillway is ~8.09 km².

2.3. Statement of the Problem

Dam breaks can result in enormous damage to downstream areas of the dam. The Baysh dam is a concrete dam established across Wadi Baysh (Figure 2a). It represents one of the largest dams in the Kingdom of Saudi Arabia. The reservoir capacity reaches ~192 million cubic meters (MCM). Many urban areas are settled downstream of the dam along the wadi course and the floodplain of the wadi (Figure 1b,c). The dam was constructed by the Ministry of Environment, Water, and Agriculture

of the KSA. There are many agriculture activities downstream of the dam site affected by floods (Figure 2b). There is likelihood of loss of human lives, urban and agriculture areas, and other economic activities if dam failure occurs. The dam of Wadi Baysh represents a threat to the urban areas located in the dam downstream, especially in the rainy seasons. The heavy rainfalls that hit the Baysh dam basin and the surrounding areas in April 2016 lasted 3 days and led to the reservoir being filled up to the spillway level (Figure 2c) and causing water to run off over the spillway (Figure 2d). This resulted in dozens of villages being inundated, the destruction of a number of vehicles and roads, and death by drowning of a number of citizens and residents (Figure 2e,f). In addition, the dam's flood gates were opened for many days to alleviate the reservoir capacity, as requested by the KSA authority (Figure 2g). The flooding led to the flow of large quantities of the runoff water into the Red Sea. A lot of media and newspapers were critical of this crisis and speculated about what would happen if the dam failed. This led us to evaluate the hydrological and hydraulic responses of the dam and reservoir under different conditions and led to the establishment of an inundation model for if the dam failed.



Figure 2. Photographs showing; (a) dam is concrete, (b) inundation of agriculture areas during the flood, (c) reservoir capacity reaching the spillway, (d) water flow over the spillway, (e) flood water invading the villages, (f) floods rendering the roads and highways impassible, and (g) water level change in the reservoir due to continuous discharge of water from reservoir (according to the KSA authority request).

3. Data Used and Methodology

3.1. Data Used in the Current Study

In the present study, different data sources were used. All datasets have been georeferenced according to UTM projection (Zone 38), WGS84 Datum. The data can be grouped in the following categories:

1. Satellite data: Landsat Operational Land Imager (OLI) images with 15-m resolution acquired in 2018 for the study area were obtained from Earth explorer website (USGS). Landsat 8 data consists of eleven bands; however, a layer stacking was done for bands (1, 2, 3, 4, 5, 6, and 7) to create an image mosaic with 30-m spatial resolution, followed by image fusion with band 8 (panchromatic 15-m resolution) to create a final mosaic with 15-m spatial resolution. In addition, a high-resolution image was used, which is available on ArcGIS program background (Google Earth image). A Digital Elevation Model (DEM) 12.5-m resolution was acquired from ALOS-PALSAR digital elevation using the Alaska Satellite Facility (the data was obtained at a time when the dam reservoir was almost empty to get an accurate measurement of reservoir volume). A DEM 30-m spatial resolution was acquired from ALOS Global Digital Surface Model (ALOS World 3D-30m), which was used to extract the drainage networks and catchments. A DEM 10-m resolution was acquired from the King Abdul Aziz City for Science and Technology (KACST), which was used to prepare the cross sections along the areas downstream of the dam to establish the inundation model.
2. Geologic map of 1:250,000-scale and topographic sheets of 1:50,000-scale for the study area, obtained from the Saudi Geological Survey, were used in the current study.
3. Rainfall stations located inside and surrounding the catchment area were identified. These include stations A004, A104, A121, N103, SA002, SA102, SA106, SA110, SA125, SA126, SA140, SA145, and SA204. Data records of these stations were collected from the Ministry of Environment, Water, and Agriculture.
4. Dam, spillway, and reservoir characteristics (dam type, height, and length; reservoir area and capacity; and spillway level, width, and height) were obtained from the Ministry of Environment, Water, and Agriculture.
5. Field investigations were carried out at the dam, reservoir, and downstream flood plain areas to collect data related to the existing impact of the flooded areas, to get information from the people in the area related to previous, current, and future problems, and to take photographs to document different situations. Furthermore, a field survey was done to collect cross sections along the downstream dam site that could be used to verify the inundation impacts at 100- and 200-year rainfall events and to validate the inundation model.

3.2. Methodology

The current study demonstrates the application of remote sensing (RS), geographic information systems (GIS), hydrologic and hydraulic models (WMS, HEC-HMS, and FlowMaster) to understand the relationship between rainfall depth and reservoir response at different scenarios (100- and 200-year rainfall return periods, and PMP). In addition to that, the goal is to determine the impact of dam failure on the downstream area by modeling the effect of the water inundation using the simplified dam break model (SMPDBK). To achieve that the following methodologies were applied.

Watershed Modeling System (WMS v. 10) [46] was used to extract drainage networks and catchment boundaries as well as to calculate their morphometric parameters with the help of DEM (30-m resolution). Application of rain frequency analysis was done using different statistical programs to determine the main statistical characteristics of each rain station record. HYdrological FRequency ANalysis (HYFRAN) software [47] was also used to establish and choose the best fit probability distribution for the records of each rainfall station followed by calculation of the rainfall depth for different return periods (100 and 200 years). In addition, the Probable Maximum Precipitation (PMP)

for each station was calculated using the Hershfield statistical method [48,49]. The global mapper program with the help of the digital elevation model (12.5-m resolution) was also utilized to create the dam height—reservoir volume relationship. Erdas Imaging (v. 14) [50] was used to establish the land use/land cover map by applying a supervised classification technique (maximum likelihood classification) on a Landsat OLI image (15-m resolution). Arc GIS (v. 10.2) [51] was used to create a soil map of the catchment areas from the geologic map and high-resolution satellite imagery. Finally, GIS was used to compile the land use/land cover map and soil map to develop a final map that was used to calculate the curve number of different land use and soil units.

The HEC-HMS (v. 4.0) [52] model was applied to estimate the hydraulic responses of Wadi Baysh sub-basins and dam spillway at three critical sites for different scenarios (100- and 200-year return rainfall periods and at the PMP event). These critical sites are considered to be vitally important locations for a number of reasons; 1) they represent the outlet locations for the three sub-catchments (B1, B2, and B3) of Wadi Baysh; 2) the critical site (C1) located at the spillway location represents the first discharge point if the water floods out of the dam; 3) critical site (C2) located at the intersection of Wadi Baysh with the King Abdel-Aziz Bridge connects many urban areas with each other (e.g., Sabya and Baysh cities). If this bridge was damaged or collapsed due to flooding, the whole area would be under risk; 4) critical site (C3) is located at the outlet of Wadi Baysh on the Red Sea where there is a big urban area located very close by (Al Qawz city). Based on a literature review [53–56] 100- and 200-year return rainfall periods were chosen in this study. In general, rainfall events ranging from 20- to 400-year return periods are considered for planning and designing based on purpose and type of structure [57]. However, regarding the lifetime of different infrastructure projects, flood-disaster mitigation projects are often designed for a 100-year return period [53,58]. In the current work, a great emphasis was applied on a 100- and 200-year return period flood in our analyses, as well for comparison of flood inundated results.

Routing analysis was taken into consideration during this study. The Flowmaster software was used to simulate the level of water height along field survey cross sections along the downstream portion of Wadi Baysh at return periods of 100 and 200 years. The simplified dam break (SMPDBK) model of WMS with the help of DEM 10-m resolution was used to establish the inundation characteristics (water elevation and water depth maps) at the dam failure time. This identifies the impact of dam failure on the downstream areas (agriculture, reclamation, and urban areas, and infrastructures). In addition, it determines the maximum water level in the reservoir that could be applied to prevent overtopping of the dam and downstream flooding.

4. Results

4.1. Catchment Delineation and their Characteristics

To develop rainfall-runoff models, detailed information of Wadi Baysh is required, including catchment topography to delineate drainage networks, catchment boundaries, flow paths, slopes and reach lengths. The WMS program with the help of DEM (30 m) was used to extract these parameters (Figure 1c). The morphometric parameters are shown in Table 1. The results were verified and modified on the basis of digital elevation models (10 and 12.5 m) and topographic maps (1: 50,000-scale). The main basin of the Wadi Baysh catchment has been divided into three sub-basins (B1, B2, and B3):

- (1) The first sub-basin (B1) represents the upstream area of the Wadi Baysh dam (critical site C1) with an area of $\sim 4744.6 \text{ km}^2$ and an average slope of $\sim 0.2859 \text{ m/m}$.
- (2) The second sub-basin (B2) represents the drainage area located downstream of the dam site until its exit point at the King Abdul Aziz Road (critical site C2, see Figure 1c) with an area of $\sim 548.5 \text{ km}^2$ and an average slope of $\sim 0.0699 \text{ m/m}$.
- (3) The third sub-basin (B3) represents the drainage area located downstream of the King Abdul Aziz Road to the Red Sea coast (critical site C3, see Figure 1c) with an area of $\sim 450.7 \text{ km}^2$ and an average slope of $\sim 0.0085 \text{ m/m}$.

Sub-basins B2 and B3 include agricultural areas and many urban centers (villages) (Figure 1b,c). The areas of sub-basins B2 and B3 were affected by flood events many times before the construction of the dam.

Table 1. Morphometric characteristics of Wadi Baysh sub-basins.

Sub-Basin	Sub-Basin Area (km ²)	Sub-Basin Length (km)	Maximum Flow Distance (m)	Sub-Basin Slope (m/m)	Maximum Flow Distance Slope (m/m)
B1	4744.6	87.42	157.12	0.2859	0.0150
B2	548.5	41.91	54.28	0.0699	0.0347
B3	450.7	46.23	53.27	0.0085	0.0033

4.2. Rainfall Analysis

The Kingdom of Saudi Arabia is classified as an arid climatic zone according to the Köppen-Geiger climate classification [44,45]. It has no permanent rivers or lakes, precipitation is low over most areas and of irregular frequency, and it has a high temperature in most months of the year. Rainfall usually occurs in winter and spring, with the exception of southwestern regions (where the Baysh basin is located), which are subjected to seasonal rain during the summer. The Southwestern area of the KSA is characterized by heavier rainfall than the rest of the Kingdom. However, sometimes rainfall comes as severe events with high precipitation rates over very short periods, causing sudden flash floods resulting in significant destruction to lives and properties.

In the current study, to determine the rainfall depth for 100- and 200-years return rainfall periods and for the Probable Maximum Precipitation (PMP), 13 rainfall stations operated by the Ministry of Environment, Water and Agriculture (stations A004, A104, A121, N103, SA002, SA102, SA106, SA110, SA125, SA126, SA140, SA145, SA204) were used (Figure 3a). The main rainfall station characteristics, the maximum daily values, and the maximum yearly values were calculated (Table 2). The maximum rainfall depth per day for each year for each rainfall station was analyzed using different probability distribution models. These probability methods were used to determine the best fit distribution curve and to estimate the rainfall depth values for 100- and 200-years return periods using HYFRAN software (Table 2).

The PMP value was estimated from the thirteen rainfall stations in this study. These stations were used to derive a PMP distribution for the Wadi Baysh sub-basins. The estimation of PMP at each rainfall station was done using the Hershfield method [48,49], described in World Meteorological Organization (WMO) Report 1045, “Manual on Estimation of Probable Maximum Precipitation” [59]. Two stations were excluded from the PMP analysis (A004 and SA145) because they give somewhat abnormal values than the adjacent stations. It was found that the rainfall depth of a 100-year return period ranges between 70.6 mm for station SA102 and 113.8 mm for station A004, the rainfall depth of a 200-year return period ranges between 74.9 mm for station SA102 and 137.1 mm for station A004, and the rainfall depth of PMP ranges from 275.9 mm for station SA125 to 356.4 mm for station SA126 (Table 2). Distribution rainfall maps for 100- and 200-years return periods and PMP values for each station were established using the kriging method in ArcGIS (v. 10.2). This method is appropriate when there are irregularly distributed sample data points such as rainfall and climatological stations [60,61] (Figure 3b,c,d). This was followed by calculating the weighted rainfall value for 100-year and 200-year return periods (for sub-basin B1, B2, and B3) and the PMP (for sub-basin B1, where the dam is located at the downstream of it) were calculated (Table 3).

Laity [62] and Pietersen et al. [63] mentioned that rainfall in most of the arid regions is variable and has limited impact on large basins. Accordingly, the Area Reduction Factor (ARF) was applied in the study area. Two ARF methods were applied to calculate the spatial reduction coefficient for each discharge sub-basin using Equation (1) [64,65] and Equation (2) [66].

$$ARF = (-6944.3 \times \ln(A) + 115731.9)^{0.4} \quad (1)$$

$$ARF = 1.4167 - 0.0852 \times \ln(A) \quad (2)$$

where ARF is the areal reduction factor and A is the catchment area (km^2). Equation (2) is applied if the catchment area is more than 133 km^2 .

Table 3 shows the different ARF values for each sub-basin. In the current study, the results of Equation (1) were used to calculate the final weighted rainfall depth of 100-year and 200-year rainfall return periods for the sub-basins (B1, B2, and B3) and PMP value (for sub-basin B1), which are shown in Table 3. These weighted rainfall values were used in establishing a hydrological model for this study.

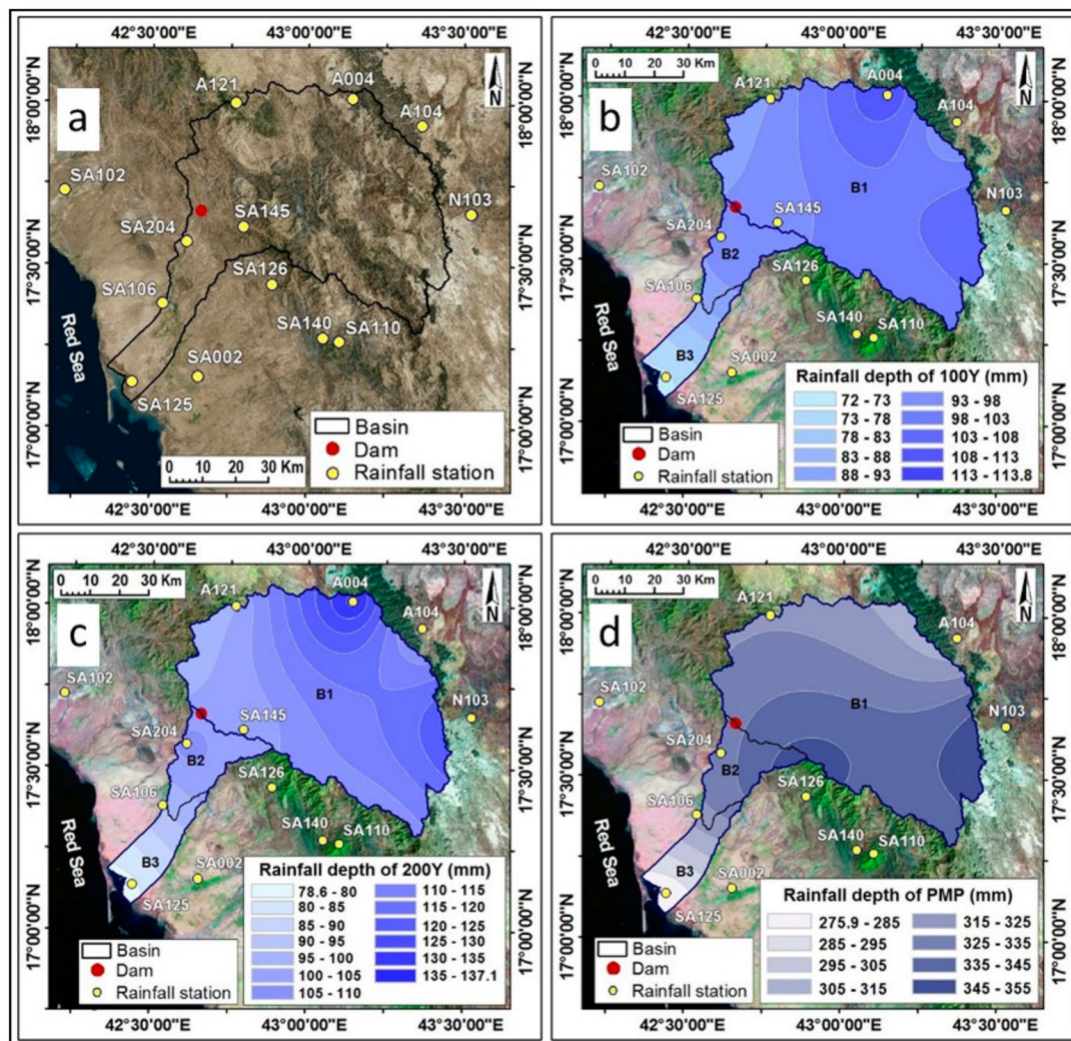


Figure 3. Presenting; (a) rainfall stations in and around Wadi Baysh basin, (b–d) rainfall depth distribution maps of 100-year and 200-year return periods and PMP respectively.

Table 2. Rainfall station characteristics including location, recording period, maximum values in a year, values of 100- and 200-year return period, probability method, and PMP values.

Station Code	Longitude	Latitude	Start/End Recording (Year)	No. of Records (Year)	Max. Daily Value (date/rain mm)	Max. Yearly Value (Year/ rain mm)	100Y (mm)	200Y (mm)	Probability Method	PMP (mm)
A004	43°08'30"	18°00'51"	1981/2017	29	3 February 1983/119	1982/283	113.8	137.1	LN (mom)	-
A104	43°21'57"	17°56'01"	1966/2017	48	7 March 1999/82	1997/566	87.8	97.4	G (mowm)	302.8
A121	42°45' 58"	17°59'55"	1965/2015	51	10 February 1968/99	1972/693.8	93.1	100.0	GEV (mowm)	323.3
N103	43°31'31"	17°39'37"	1966/2016	50	25 March 1974/130.5	1992/317.1	113.4	132.8	GEV (mowm)	361.7
SA002	42°39'10"	17°09'25"	1965/2018	48	13 April 2016/96	2016/217	81.4	90.7	G (mowm)	298.0
SA102	42°13'14"	17°43'32"	1966/2005	39	29 July 1988/68	1979/192.9	70.6	74.9	N (mowm)	309.2
SA106	42°32'16"	17°22'54"	1967/2018	44	13 April 2016/84	1967/397	88.9	95.6	GEV (mowm)	321.7
SA110	43°06'21"	17°16'01"	1960/2017	55	27 November 2008/84	1995/1041.5	90.1	93.9	GEV (mowm)	323.0
SA125	42°26'32"	17°08'18"	1967/2018	49	13 April 2004/66.4	1997/245.5	72.0	78.6	GEV (mowm)	275.9
SA126	42°53'15"	17°26'26"	1966/2017	52	19 February 1968/96	1978/1404	98.5	105.0	GEV (mowm)	358.4
SA140	43°03'07"	17°16'40"	1967/2018	45	20 June 1970/99	2006/1175.7	101.2	110.3	G (mowm)	304.6
SA145	42°47'40"	17°37'06"	1966/2017	43	5 December 1972/99	1972/1441.9	94.6	99.7	N (mowm)	-
SA204	42°36'45"	17°34'21"	1979/2012	20	8 August 2003/97.5	2005/327.7	97.6	107.9	G (mowm)	330.3

Max. = maximum; LN (mom)= LogNormal (method of moments); G (mowm)= Gumbel (method of w. moments); GEV (mowm) = GEV (method of w. moments); N (mowm) = Normal (method of w. moments); PMP = Probable Maximum Precipitation.

Table 3. Weighted rainfall depth for each sub-basin extracted from rainfall distribution maps (100- and 200-year return period and PMP), the areal reduction factor values of different methods, and final weighted rainfall depth after applying the area reduction factor values (Equation (1), Alexander method).

Sub-Basin	Sub-Basin Area (km ²)	Weighted Rainfall Depth (mm)			ARF Value According to Various Methods		Rainfall Depth After Using (ARF) (mm)		
		100 Year	200 Year	PMP	Riyad Standard (%)	Alexander (%)	100 Year	200 Year	PMP
B1	4744.6	100.4	111.8	333.3	69.6	79.8	80.2	89.3	266.1
B2	548.5	94.7	102.8	-	87.9	87.7	83.0	90.1	-
B3	450.7	80.4	87.4	-	89.6	88.3	71.0	77.2	-

4.3. Rainfall-Runoff Modeling

The study area has a lack of measured flood flow data. Inflow hydrographs of each sub-basin have been estimated using rainfall-runoff modeling. In the current study, HEC-HMS hydrological modeling software has been used. A model of the catchment is constructed by separating the hydrological cycle into manageable pieces and creating boundaries around the watershed of interest. Any mass or energy flux in the sequence can then be represented with a mathematical model. In most cases, several model choices are available for representing each flux. Each mathematical model included in the software is suitable in different environments and under different conditions based on the catchment characteristics, the local climate, and the objectives of the study. The methods are chosen to represent the hydrological response of the Wadi Baysh sub-catchments.

SCS Curve Number Loss Method

To evaluate the hydraulic response of each sub-basin, different equations were utilized. Various steps were applied to calculate the peak discharge and runoff values included. First, rainfall losses were estimated, which represents the amount of precipitation that will not runoff (e.g., water that is intercepted and transpired by vegetation, water losses due to evaporation, and water losses by infiltration downwards). The HEC-HMS model using the SCS Curve Number loss method considers all previously mentioned losses. To calculate these losses the initial abstraction (I_a), percentage of impervious surfaces of the basin, and curve number (CN) value are required. The CN depends on both land use/land cover and soil type inside each drainage basin. The SCS-CN model estimates effective rainfall value (P_e) (direct runoff) as a function of cumulative precipitation (P), soil cover and land use (weighted CN value for the basin), initial abstraction (I_a), and maximum retention (the maximum effort for soil moisture) (S_r) (see Equation (3), (4), (5), and (6) [52,67]). In general, CN values range from 100 (for water bodies) to approximately 30 for permeable soils with high infiltration rates.

$$P_e = (P - I_a)^2 / (P - I_a + S_r) \quad (3)$$

$$I_a = 0.2S_r \quad (4)$$

$$P_e = (P - 0.2S_r)^2 / (P + 0.8S_r) \quad (5)$$

$$S_r = (25400 - 254CN) / (CN) \quad (6)$$

where P_e is the direct runoff (mm); P is the rainfall for different return periods (mm); I_a is the initial loss (mm) (amount of water loss before the occurrence of the runoff, such as filtration and suspended rain on the plants); S_r is the maximum retention (cm) (maximum effort for soil moisture, which is calculated from the curve number); and CN is the curve number.

Furthermore, the SCS method requires lag times to be calculated for each sub-catchment. Lag time (T_{lag}) is defined as the time from the center of mass of excess rainfall to the hydrograph peak [52]. The SCS lag time equation has been adopted since it provides consistency with the SCS UH model being used (see Equation (7)). A peak discharge (q_p) is calculated for each sub-basin for different return periods (see Equation (8)). The time to peak (T_p) can also be calculated (see Equation (9)).

$$T_{LAG} = \frac{L^{0.8}[S_r + 1]^{0.7}}{1900 \sqrt{Y}} \quad (7)$$

$$q_p = \frac{0.208AQ}{T_p} \quad (8)$$

$$T_p = \Delta t/2 + T_{LAG} \quad (9)$$

where T_{LAG} is the Lag Time (hour); L is the maximum flow distance (ft); Y is the basin slope (%); qp is the peak discharge (m^3/s); A is the basin area (km^2); T_p is the time to peak (hour); and Δt is the duration of the design storm water.

In the current study, various data sources were used including satellite imagery, soil maps, and superficial geology maps of the area. The land use/land cover map was extracted from a Landsat OLI image (15-m resolution) using a supervised classification technique. A soil map was created from the analysis of the geologic map and high-resolution satellite image. A final map was developed by a compiling of the land use/land cover map and soil map using ArcGIS 10.2 (Figure 1b). Seven different CN values were selected for the Wadi Baysh sub-catchments. CN values of 88, 82, 80, 78, 72, 69, and 63 were assigned to urban areas, igneous and metamorphic mountainous/rocky areas, sabkha areas, sedimentary rocks (limestone and sandstone rocks), agriculture areas, alluvium deposits, and sand dune areas, respectively. Eventually, weighted curve numbers for each sub-catchment (B1, B2, and B3) were calculated as 81.1, 77.1, and 70.0, respectively.

4.4. Height-Storage Reservoir Curve

In the current study, HEC-HMS was used to generate the inflow hydrographs to the three sub-basins (B1 (dam basin), B2, and B3) and to route the flow through the dam reservoir. To achieve that the reservoir characteristics were entered into the model for sub-basin B1. Based on the digital elevation model (12.5 m) and the data available for the dam characteristics, the aerial extent of the reservoir at the spillway level at a pool of ~62 m covers ~8.09 km^2 and at the dam crest level (~74 m) reaches ~10.09 km^2 . This is shown in Figure 4a. Similarly, the dam height storage curve was extracted using the digital elevation model (12.5 m). The relationship between the dam height and reservoir volume represents one of essential inputs when dealing with dams in hydraulic and hydrological models, as shown in Figure 4b. The dead reserve, spillway level, and dam crest are shown in Figure 4b.

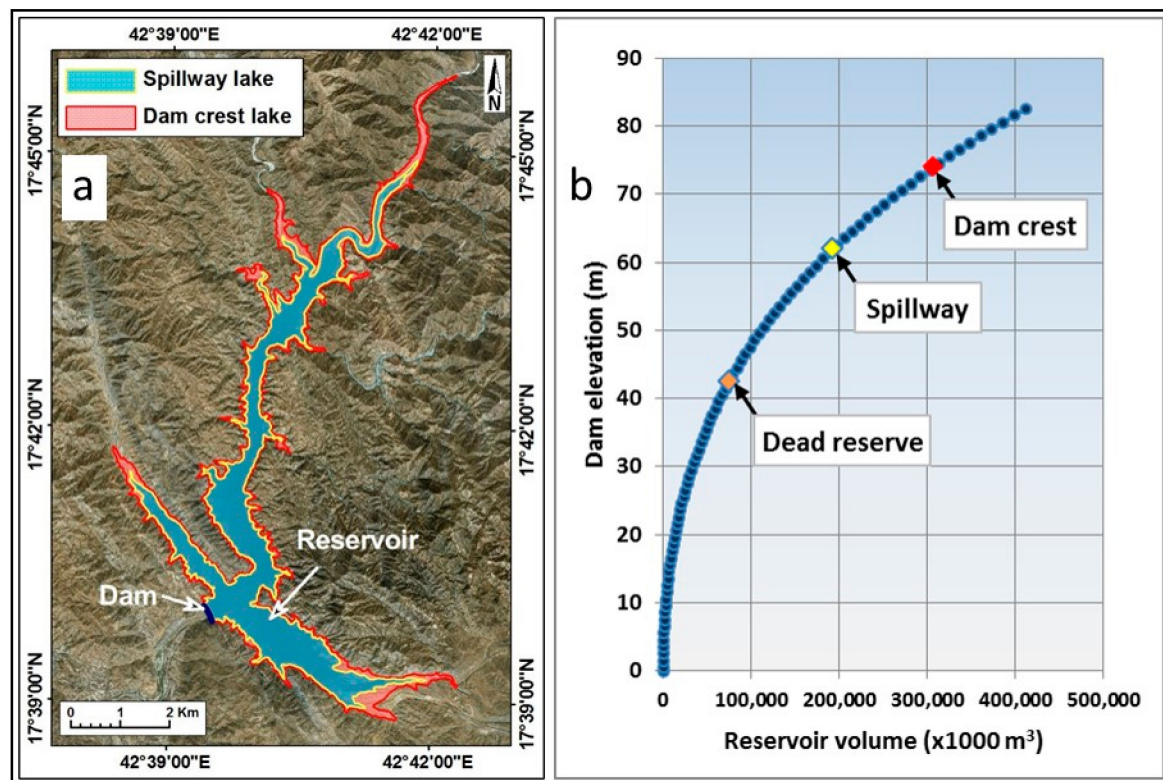


Figure 4. Showing: (a) outlines of the dam crest and spillway water levels of the Wadi Baysh reservoir, (b) dam height reservoir volume curve.

5. Preparation of the Hydrological Model using HEC-HMS

The hydrological model of the current study was prepared using the HEC-HMS program. This model includes several deductive methods for calculating peak discharge and runoff volume for each sub-basin. Different parameters were entered into the HEC-HMS program. The overflow structures include level and length of spillway and dam crest in the model. The bottom outlets were ignored as these will remain closed until the reservoir is required to be emptied following a flood event, according to the Ministry of Environment, Water and Agriculture requirements. The initial operation of the hydrological model was prepared. Two stages were applied in the current situation:

- (1) Evaluating the hydrologic response of the three sub-basins (B1, B2, and B3) for a 100-year and 200-year rainfall return period neglecting the effect of the dam (dam is not present).
- (2) Evaluating the hydrologic response with the dam presence at 100-year and 200-year rainfall return periods (for sub-basins B1, B2, and B3) and at the PMP event (for sub-basin B1). In this stage, routing through the reservoir was applied. In addition, different scenarios were analyzed to understand the impact of the reservoir on the hydraulic response in different situations (regarding sediment volume and water in the reservoir).

5.1. Stage I: No Dam Present

The peak discharge of drainage sub-basins was calculated (neglecting the dam effect). The rainfall weighted values for sub-basins were determined from the rainfall distribution maps for a 100-year and 200-year return period after the application of area reduction factor (Table 3). The results of this stage for the three basins are presented in Table 4.

Table 4. Flood results of different drainage basins (no dam effect).

Sub-Basin	Lag Time (Hour)	Peak Discharge (m ³ /s)		Flood Volume x 1000 m ³	
		100 Year	200 Year	100 Year	200 Year
B1	8.5	3465	4176	174,066	208,657
B2	8.3	355	414	17,708	20,549
B3	28.6	49	60	6691	8438

5.2. Stage II: Dam and Reservoir Effect on the Hydraulic Responses

In this stage, all data required to represent the Wadi Baysh dam and reservoir within the hydrological model were inserted. This will help in estimating the current status of the flood behavior for 100-year and 200-year return periods. Before the hydrological model was run, sediment volumes and sediment heights inside the reservoir were calculated. The Baysh dam was built in 2009, but the sediment volume was estimated in the beginning of the year 2019 (which represents ten years since dam construction) to be ~14.95 Million Cubic Meters (MCM) with a sediment height of ~20.9 m from the base of the dam (Wadi level). After 20 years from the dam construction (in 2029), sediment volume and height are estimated to be ~29.9 MCM and ~28.5 m respectively; after 30 years from the dam construction (in 2039), sediment volume and height are estimated to be ~44.9 MCM and ~34.1 m respectively; after 40 years from the dam construction (in 2049), sediment volume and height are estimated to be ~59.8 MCM and ~36.6 m respectively; and after 50 years from the dam construction (in 2059), sediment volume and height are estimated to be ~74.75 MCM and ~42.5 m respectively. The hydrological model was run and the results of the different scenarios (cases) were evaluated to determine the hydraulic response of the dam and spillway (Table 5, Figure 5).

Table 5. Results of different scenarios to describe the dam, reservoir, and spillway responses, dam crest height 74m, and spillway level height 62m.

Case No.	Return Period	Sediment Volume	Total Reservoir Volume *	Maximum Water Height	Water Depth in the Spillway	Critical Site (1)		Critical Site (2)		Critical Site (3)	
	Year	(* 1000 m ³)	(* 1000 m ³)	(m)	(m)	Q (m ³ /s)	V (m ³)	Q (m ³ /s)	V (m ³)	Q (m ³ /s)	V (m ³)
Case (1)	100	14,950	14,950	61.4	0.0	0.0	0.0	354.6	17,708	372.6	24,586
	200	14,950	14,950	63.7	1.7	467.7	29,548	487.4	51,235	543.2	59,413
Case (2)	100	14,950	192,000	67.5	5.5	2,858	173,134	3,087	190,843	3,104	197,630
	200	14,950	192,000	68.2	6.2	3,505	207,722	3,781	228,275	3,800	236,563
Case (3)	100	14,950	98,445	65.5	3.5	1,403	79,580	1,495	97,329	1,532	103,969
	200	14,950	98,445	66.5	4.5	2,088	114,169	2,238	134,775	2,277	142,887
Case (4)	100	74,750	74,750	64.8	2.8	955	55,885	1,008	73,622	1,051	80,286
	200	74,750	74,750	65.9	3.9	1,646	90,473	1,753	111,070	1,798	119,203

* Total reservoir volume means the volume before each flood event.

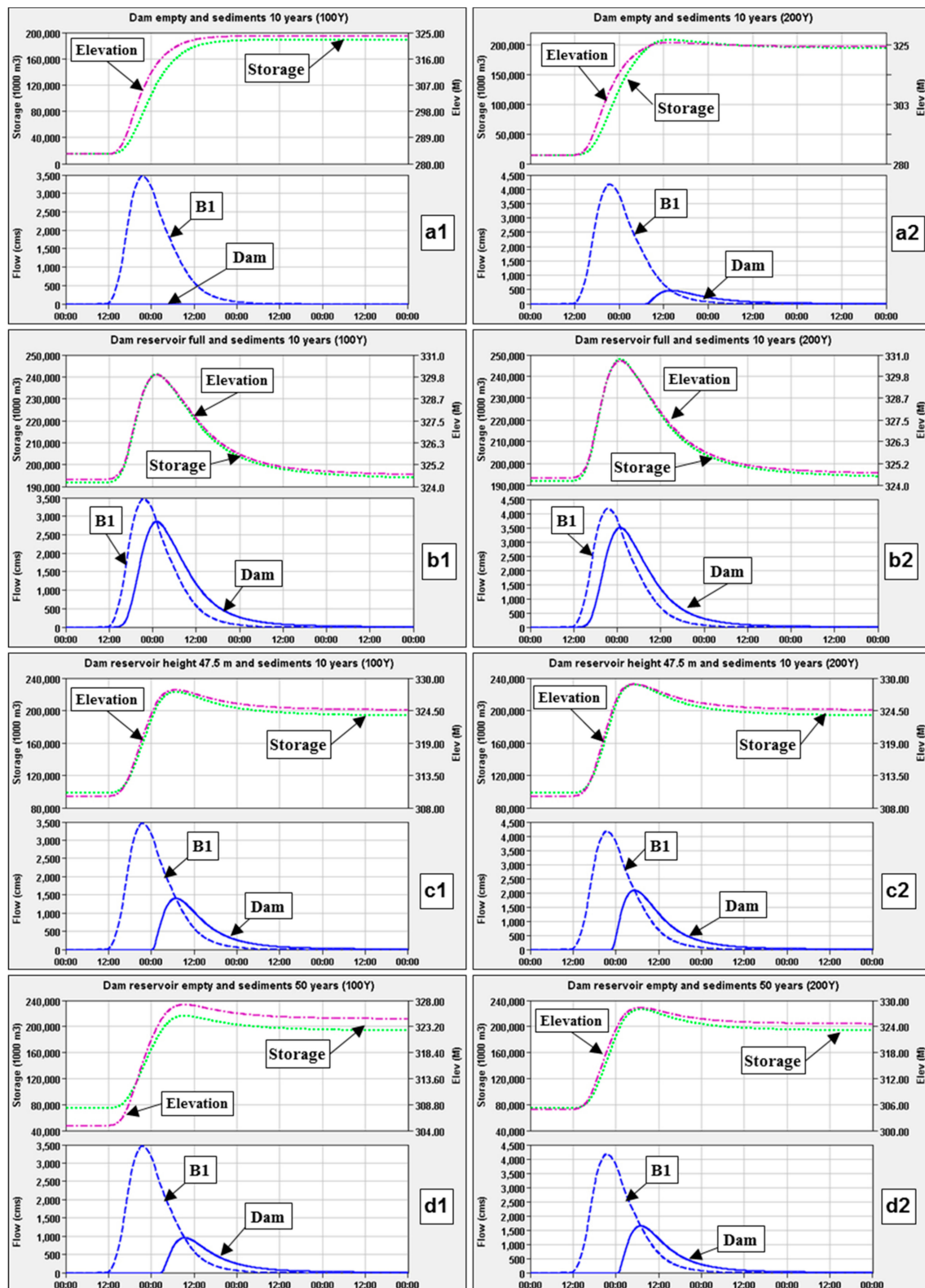


Figure 5. Flood hydrographs of Wadi Baysh dam for 100- and 200-year return periods; (a1, a2) dam empty and sediment of 10 years; (b1, b2) dam reservoir full and same sediment; (c1, c2) dam reservoir height 47.5 m and same sediment; (d1, d2) dam reservoir empty and sediment of 50 years. Note that B1 is the sub-basin located upstream of the dam site.

Case (1): In this case, the reservoir is assumed to be empty and the sediment volume equivalent to 10 years from the dam construction. Using the rainfall depth for return periods (100 and 200 years), the results of the hydraulic model are presented in (Table 5 and Figure 5a1,a2). In this scenario the reservoir capacity to hold the floodwater accumulated due to the fact that the possible rainstorm for the 100-year return period is adequate, while water height inside the spillway is up to ~1.7 m when the model is run with a return period of 200 years.

Case (2): In this case, the reservoir is assumed to be full to the spillway level (as shown in Figure 2b, d) and the sediment volume equivalent to 10 years from the dam construction. The results of the hydrological model for 100- and 200-year return periods are shown (Table 5 and Figure 5b1,b2). It was found that at a return period of 100 years the water height inside the spillway is up to ~5.5, while there will be a rise of water level above the base of the spillway up to ~6.2 m with a 200-year return period.

Case (3): In this case, the reservoir is assumed to be at the height of 47.5 m. Before it reaches this level, the water in the reservoir spills out of the reservoir through the spillway. This new reservoir level represents the level of the reservoir after the KSA authority forced the dam's manager to discharge its water to that level (Figure 2e). The sediment volume is equivalent to 10 years from the dam construction. The reason for that is to save the dam integrity, to protect the dam body from overtopping, and to decrease the flood impact on the downstream urban and agriculture areas. In this case, the hydrological model indicated that for a 100-year return period the water height inside the spillway will reach ~3.5 m, while for a 200-year return period the height of the water within the spillway reaches ~4.5 m (Table 5 and Figure 5c1,c2).

Case (4): In this case, the reservoir is assumed to be empty and the sediment volume is equivalent to 50 years from the dam construction (the total volume of the sediment estimated to be ~74.8 Million Cubic Meters (MCM) and the height of the sediment behind the dam body will be ~42.5 m). Accordingly, by running the hydraulic model, it was found that for a 100-year return period the flood water will reach a height of ~2.8 m inside the spillway. While in the event of a 200-year return period, the water height will reach ~3.9 m inside the spillway (Table 2 and Figure 5d1,d2).

In addition, the peak discharge and runoff volume were estimated at three critical sites including critical site C1 at the spillway location, critical site C2 at the intersection of Wadi Baysh with the King Abdel-Aziz Bridge, and critical site C3 at the outlet of Wadi Baysh on the Red Sea (Figure 1c). The peak discharge and water volume at these three locations for return periods of 100 and 200 years are shown in Table 5. The results indicated that the dam reservoir would provide very adequate performance under 100-year and 200-year return periods. The height of the water inside the spillway ranges from 0 to ~5.5 m based on a 100-year return period and from ~1.7 to ~6.2 m based on a 200-year return period without any danger to the dam body. The discharge values at the critical site C1 range from 0 to ~2858 m³/s, at C2 it ranges from ~354.6 to ~3087 m³/s, and at the critical site C3 it ranges from ~372.6 to ~3104 m³/s for a 100-year return period. However, for a 200-year return period, the discharge value at the critical site C1 ranges from ~467.7 to ~3505 m³/s, at the critical site C2 it ranges from ~487.4 to ~3781 m³/s, and at the critical site C3 it ranges from ~543.2 to ~3800 m³/s.

Furthermore, evaluations of the level of water at 100- and 200-year rainfall return periods along the downstream Wadi Baysh section were done. Results of the case 2 scenario were used where the level of water above the base of the spillway is ~5.5 and ~6.2 m for 100- and 200-year return periods. A ground survey was conducted in the field and six cross sections were established (Figure 6). Observed catchment rainfall and flow data provide the basis for model calibration and validation. It was originally intended to base the model calibration on available historical rainfall and water level records for the study area. Flood inundation that previously occurred in the area (e.g., Figure 1b,e,f) was used to validate the flood inundation along each ground survey cross section (Figure 7), as well as the historical flood data that were collected from the people in the area who dwell downstream of Wadi Baysh. Our findings indicated that there is a reasonable agreement of the level of floods that happened previously with the 100-year return period floods.

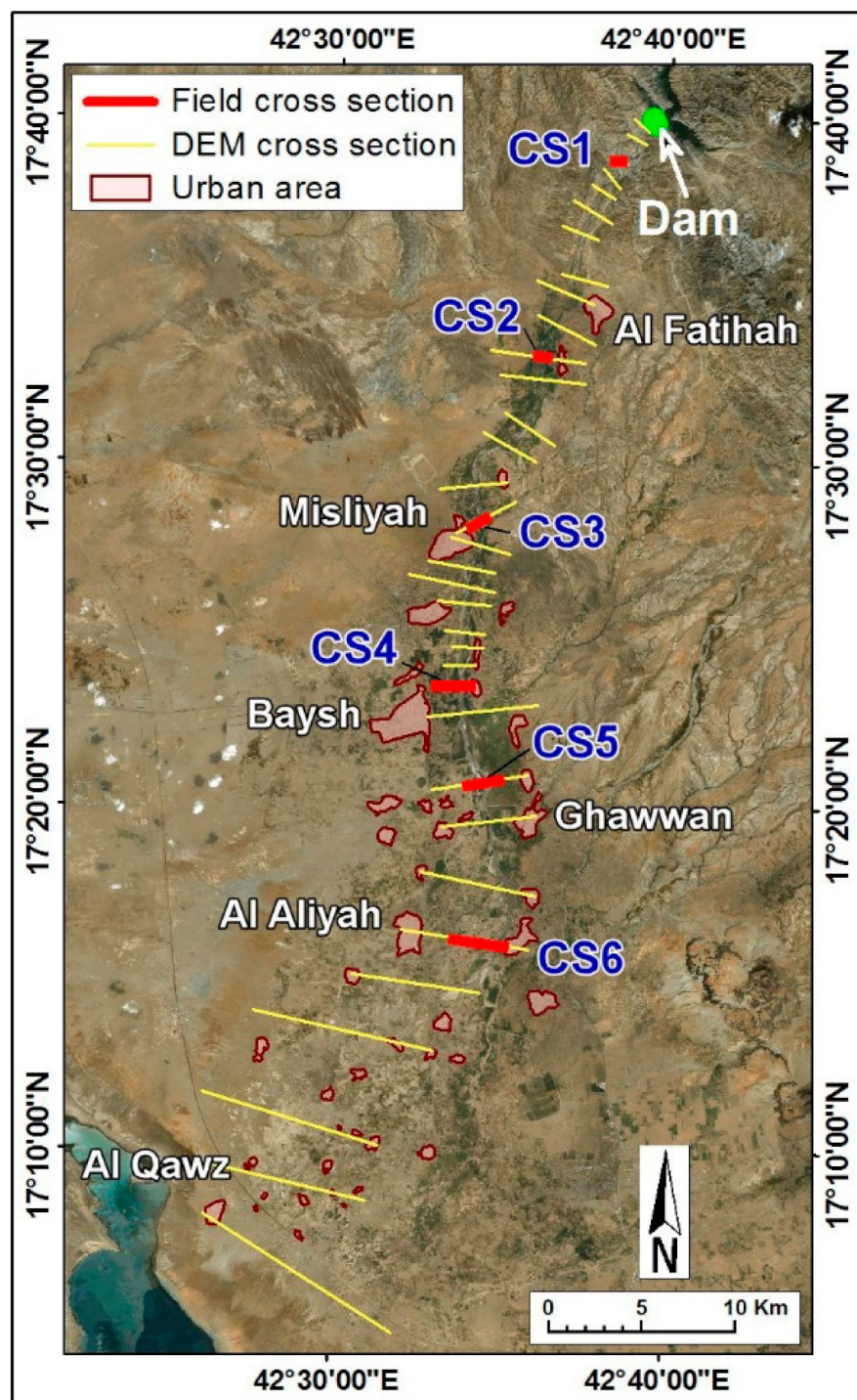


Figure 6. Locations of cross sections collected from the field.

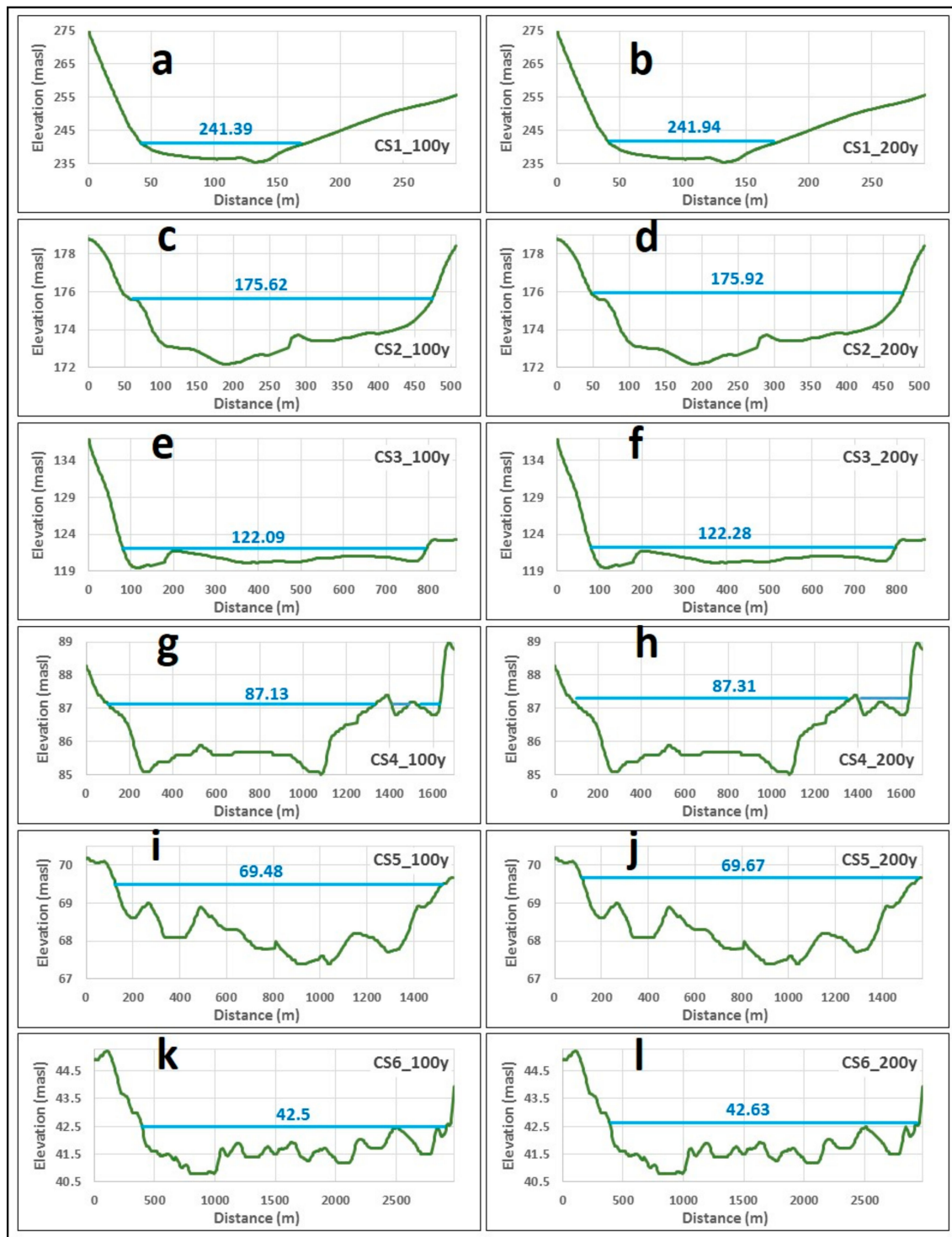


Figure 7. Ground survey results showing: (a–l) cross sections used to verify the Simplified Dam Break model (SMPDBK) and to find inundation at 100 and 200 years.

The Manning Equation (6) was used to estimate the water level at 100- and 200-year return periods as shown in (Figure 7). Results indicated that the wadi section in the downstream area is heterogeneous and many tributaries are developed.

$$Q = \frac{R^{2/3} S^{1/2}}{n} A \quad (10)$$

where Q is the peak discharge (m^3/s); R is the hydraulic radius; S is the wadi slope (m/m); n is the Manning coefficient; and A is the flow cross section area (m^2). Results indicated that if the wadi section is located downstream of the dam site, the urban and agriculture areas will not be impacted by the flood problems at 100- and 200-year return periods.

5.3. Maximum Rainfall Causing Flooding without the Overtopping of the Dam

Rainfall values are usually used for the Maximum Probable Precipitation (PMP) to ensure that the water is not overtopping the dam body. The PMP value must be used to protect the dam at the worst conditions. For that reason, the spillway has to be designed to discharge the flow from such storms. The weighted PMP value obtained for sub-basin (B1) is 268 mm, which indicates that the peak discharge of this PMP would be overtopping the dam body. The PMP value of sub-basin (B1) exceeds a 20,000-year return period. The Baysh dam is characterized by the presence of a large spillway located along the dam structure (10 m high and 112 m wide). It is essential to calculate the expected maximum rainfall depth that could be imposed on the dam sub-basin causing a flow from the spillway without overtopping the dam body. Three scenarios were evaluated:

- (1) the reservoir is empty (no water),
- (2) the reservoir is full up to the spillway level (~62 m), and
- (3) the water in the reservoir is up to ~47.5 m height (lower than the spillway level).

The hydrological model was run and the results recorded for each case. For the first premise where the reservoir is empty, it was found that the rain depth will be ~172 mm, which represents a return period above 10,000 years, causing a peak discharge of ~8980 m^3/s , and the runoff water is ~555.1 MCM. For the second premise, the dam reservoir is full up to the spillway level, and it was found that the rainfall depth will be ~158 mm, which represents a return period above 10,000 years, causing a peak discharge of ~8948 m^3/s , and the runoff water is ~493.8 MCM. For the third premise, the dam reservoir is full up to a height of 47.5 m, and it was found that the rainfall depth will be ~168 mm, which represents a return period above 10,000-years, causing a peak discharge of ~8947 m^3/s , and the runoff water is ~537.5 MCM.

5.4. Simulation of the Situation at Dam Failure, if the Reservoir is Full

In the current section, dam failure due to overtopping was simulated. Many urban and agricultural areas are located downstream of the dam site, as shown in Figure 1b,c and 6. To evaluate and mitigate the severe impact of flood water on urban and agricultural areas at the dam failure time, an inundation model was established using the Simplified Dam Break (SMPDBK) model of WMS. This was carried out using the intersection of water elevations computed from the result of the SMPDBK model and the ground elevations. Dam failure due to an unprecedented flood event will have enormous potential threats to infrastructure and human life in this area. DEM 10-m spatial resolution was used to build the SMPDBK model. The cross sections that were extracted from the DEM 10-m and used to establish flood inundation areas using the SMPDBK model were calibrated and validated using ground survey cross sections (Figures 6 and 7). It was found that there is a good match between the cross sections developed from the DEM and ground survey cross sections. That gives good confidence in the results of the SMPDBK model. The wadi cross section width was measured as follows: 133 m and 138 m for CS1, 417 m and 430 m for CS2, 714 m and 718 m for CS3, 1426 m and 1538 m for CS4, 1393 m and 1454 m for CS5, and 2520 m and 2542 m for CS6 for 100- and 200-year return period floods respectively (Figure 7). Furthermore, the depth of water along the ground survey sections were evaluated as follows: for CS1, water depths are 5.9 m and 6.5 m; for CS2 water depths are 3.5 m and 3.8 m; for CS3 water depths are 2.6 m and 2.8 m; for CS4 water depths are 2.1 m and 2.3 m; for CS5 water depths are 2.1 m and 2.3 m; and for CS6 water depths are 1.7 m and 1.8 m for 100- and 200-year return period floods respectively (Figure 7). Results indicated that water depth increased along the vicinity of the dam site where the wadi width is small and water depth decreased westward toward the Red Sea

coast due to the increasing width of the Wadi Baysh flood plain. The inundation map was prepared with the SMPDBK model. The results indicate that there is a high risk to the inundated flood zone. The model produces the water elevation along the inundated zone, the depth of inundation, and the inundation hazard categories along the downstream zone (Figure 8a–c). The results of the inundation map show a robust geographic correlation with historical flash flood events in the study area (data records of inundated areas from data collected by the civil defense agency and from local people in the area, from before dam construction). Furthermore, the model was calibrated and validated using real observed data. Water level along the inundation zone ranges from 96 to 3.8 m above sea level (Figure 8a). The inundation model covers a vast area along the downstream floodplain (see Figure 8b,c). The inundated hazard map indicates water depth ranges from 0 to 16.8 m (Figure 8b). It could be classified into six main classes as follows: less than 1 m (very low hazard), 1 to 2 m (low hazard), 2 to 3 m (moderate hazard), 3 to 6 m (high hazard), and more than 6 m (very high hazard) (Figure 8c). This hazard map was carried out in relation to the urban areas along the study area where most of the buildings are one story (height up to 3 m) and some are two story buildings (up to 6 m height). Due to the presence of these buildings, there is ability for people to be safe if they are above the roof of the first story buildings. However, this hazard zone map could be deadly if the water is above 1 m for people on farms and driving vehicles.

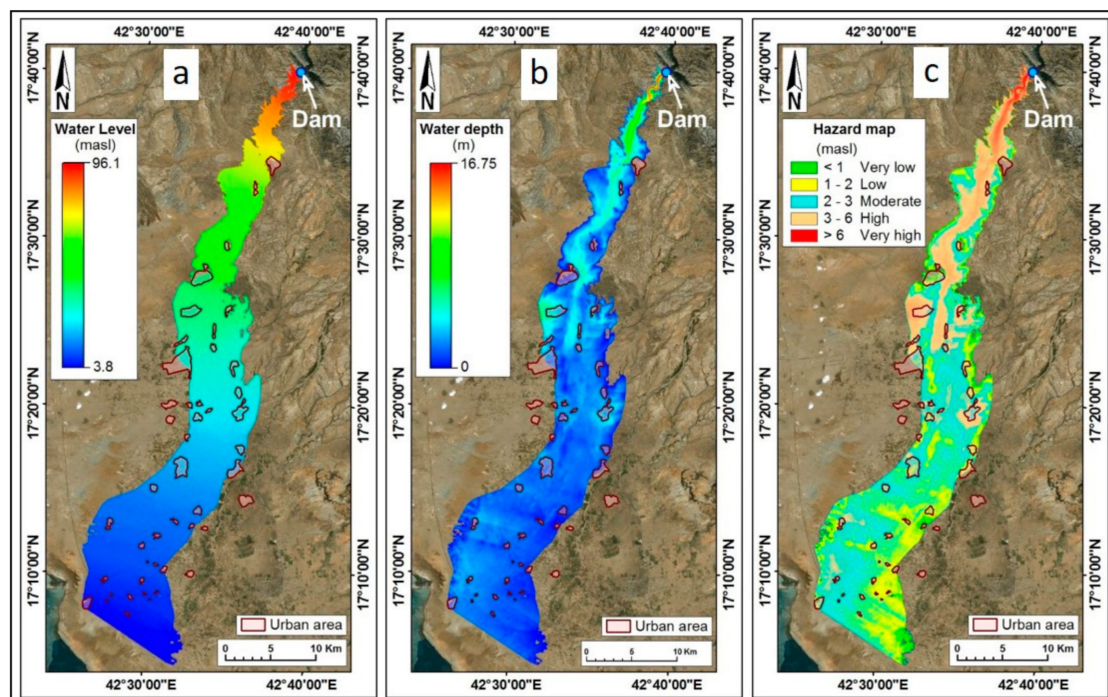


Figure 8. SMPDBK model results showing, (a) water elevation across the inundated zone, (b) water depth along the inundated section of the downstream area, (c) inundation hazard map along the study area.

6. Discussion and Conclusions

Recently, the Kingdom of Saudi Arabia has faced extraordinary rainfall (frequency and intensity) events. Reliable prediction of runoff and establishing different hydrologic and hydraulic models are very crucial for prediction of flooding events for critical wadis. The development of a hydraulic model for the downstream areas of dam sites is an essential task for decision makers and planners to prevent urban and agricultural areas from experiencing the adverse impact of floods. The current HEC-HMS model for Wadi Baysh with different scenarios indicated that the dam can hold and discharge the water flow under different situations at rainfall return periods of 100 and 200 years. Water depth in the dam spillway will be between 0 and ~5.5 m for 100 years and between ~1.7 and ~6.2 m for 200 years

at different scenarios with no overtopping of the dam. The peak discharge at the three critical sites (C1, C2, and C3) was estimated showing that the maximum discharge is $\sim 2858 \text{ m}^3/\text{s}$ at critical site C1 (spillway location), $\sim 3087 \text{ m}^3/\text{s}$ at critical site C2, and $\sim 3104 \text{ m}^3/\text{s}$ at critical site C3 for a 100-year return period. The maximum discharge is $\sim 3505 \text{ m}^3/\text{s}$ at critical site C1, $\sim 3781 \text{ m}^3/\text{s}$ at critical site C2, and $\sim 3800 \text{ m}^3/\text{s}$ at crucial site C3 for a 200-year return period. Accordingly, long-term precautionary measures need to be considered for a return period of 200 years. Rehabilitation of the wadi needs to be implemented for the first section from critical site C1 to critical site C2 (at the intersection of Wadi Baysh with the King Abdel-Aziz bridge) to accommodate a discharge of $\sim 3750 \text{ m}^3/\text{s}$ followed by a discharge of $\sim 3800 \text{ m}^3/\text{s}$ from critical site C2 to critical site C3 (at the outlet of Wadi Baysh on the Red Sea). In addition, the results showed that the dam reservoir could absorb a rainstorm up to $\sim 172 \text{ mm}$ occurring above sub-basin B1 if the reservoir is empty. However, the maximum water flow of the dam spillway will be $\sim 8950 \text{ m}^3/\text{s}$ when the rainfall above Wadi Baysh sub-basin B1 is $\sim 158 \text{ mm}$, where the water level in the dam reservoir is initially up to the spillway level.

The inundated model using SMPDBK indicated that a catastrophic problem could occur at the time of dam failure where the water depth could reach 16.75 m height above ground level in some areas. Accordingly, a vulnerability evaluation of the downstream portion of the Wadi Baysh dam to floods at dam failure time is very essential. Many urban and agricultural areas will be under high risk of flooding. Model verification has been done due to historical flash flood events and the ground survey cross sections. A disaster and emergency management program needs to be implemented in the KSA to prevent massive loss of lives. The model results showed that flood inundation is unequivocally likely to impact agricultural and urban areas, as well as the infrastructure along the downstream area. The results of this model will have great benefit to the decision makers, policymakers, civil defense, and urban planners to support and help them to understand the extent of the inundated areas and to make the right decision. Modelling results also generate crucial information needed to establish a mitigation strategy to avert hazards associated with flash floods due to dam failure. To control and reduce the effect of flash floods in this area due to potential dam failure, several mitigation measures can be applied such as (i) establishing a flood prevention program, (ii) conducting intensive dam inspection programs, (iii) designing adequate drainage systems for the area downstream of the dam site, (iv) establishing an effective warning system that could inform people during extreme events to evacuate and (v) controlling and managing the water in the dam reservoir before and during the rainy season.

Author Contributions: Conceptualization, M.M.A., and A.M.Y.; Data curation, A.M.Y., and H.M.A.; Formal analysis, M.M.A., A.M.Y., N.H.M., E.A., H.M.A., and N.S.A.; Investigation, M.M.A., and N.S.A.; Methodology, A.M.Y., E.A., H.M.A., and N.S.A.; Software, M.M.A., E.A., A.M.Y.; Writing—original draft, M.M.A., A.M.Y., N.H.M., and E.A.; Writing—review & editing, A.M.Y. and N.H.M. All authors have read and agreed to the published version of the manuscript.

Funding: This research received no external funding.

Acknowledgments: The authors highly appreciate the constructive comments and suggestions provided by the anonymous reviewers in improving the quality of this work.

Conflicts of Interest: The authors declare no conflict of interest.

References

1. Alexander, D.E. Natural disasters, a framework for research and teaching. *Disasters* **1991**, *15*, 209–226. [[CrossRef](#)] [[PubMed](#)]
2. Alexander, D.E. *Natural Disasters*; Kluwer Academic Publishers: London, UK, 1993.
3. Zwenzner, H.; Voigt, S. Hydrology and Earth System Sciences Improved estimation of flood parameters by combining space-based SAR data with very high-resolution digital elevation data. *Hydrol. Earth Syst. Sci.* **2009**, *13*, 567–576. [[CrossRef](#)]
4. Bathrellos, G.D.; Karymbalis, E.; Skilodimou, H.D.; Gaki-Papanastassiou, K.; Baltas, E.A. Urban flood hazard assessment in the basin of Athens Metropolitan city, Greece. *Environ. Earth Sci.* **2016**, *75*, 319. [[CrossRef](#)]

5. Habibi, H.; Nasab, A.R.; Norouzi, A.; Nazari, B.; Seo, D.-J.; Muttiah, R.; Davis, C. High Resolution Flash Flood Forecasting for the Dallas-Fort Worth Metroplex. *J. Water Manag. Model.* **2016**. [CrossRef]
6. Rahmati, O.; Zeinivand, H.; Besharat, M. Flood hazard zoning in Yasooj region, Iran, using GIS and multi-criteria decision analysis. *Geomat. Natural Hazards Risk* **2016**, *7*, 1000–1017. [CrossRef]
7. Razavi Termeh, S.V.; Kornejady, A.; Pourghasemi, H.R.; Keesstra, S. Flood susceptibility mapping using novel ensembles of adaptive neuro fuzzy inference system and meta-heuristic algorithms: Ant colony optimization, genetic algorithm, and particle swarm optimization. *Sci. Total Environ.* **2018**, *615*, 438–451. [CrossRef]
8. Youssef, A.M.; Pradhan, B.; Gaber, A.F.D.; Buchroithner, M.F. Geomorphological hazards analysis along the Egyptian Red Sea Coast between Safaga and Quseir. *Nat. Hazards Earth Syst. Sci.* **2009**, *9*, 751–766. [CrossRef]
9. Kjeldsen, T.R. Modelling the impact of urbanization on flood frequency relationships in the UK. *Hydrol. Res.* **2010**, *41*, 391–405. [CrossRef]
10. Sene, K. *Flash Floods: Forecasting and Warning*; Springer: Dordrecht, The Netherlands, 2013; p. 395.
11. Tehrany, M.S.; Pradhan, B.; Jebur, M.N. Flood susceptibility analysis and its verification using a novel ensemble support vector machine and frequency ratio method. *Stoch. Environ. Res. Risk Assess.* **2015**, *29*, 1149–1165. [CrossRef]
12. Fowler, H.J.; Cooley, D.; Sain, S.R.; Thurston, M. Detecting change in UK extreme precipitation using results from the climateprediction.net BBC climate change experiment. *Extremes* **2010**, *13*, 241–267. [CrossRef]
13. Coumou, D.; Rahmstorf, S. A decade of weather extremes. *Nat. Clim. Chang.* **2012**, *2*, 491–496. [CrossRef]
14. Kundzewicz, Z.W.; Kanae, S.; Seneviratne, S.I.; Handmer, J.; Nicholls, N.; Peduzzi, P.; Mechler, R.; Bouwer, L.M.; Arnell, N.; Mach, K.; et al. Flood risk and climate change: Global and regional perspectives. *Hydrol. Sci. J.* **2014**, *59*, 1–28. [CrossRef]
15. Dawson, R.J.; Gosling, S.; Chapman, L.; Darch, G.; Watson, G.; Powrie, W.; Bell, S.; Paulson, K.; Hughes, P.; Wood, R.; et al. Chapter 4: Infrastructure. In *UK Climate Change Risk Assessment 2017 (CCRA 2017)*; Adaptation Sub-Committee (ASC) of the Committee on Climate Change: London, UK, 2016.
16. Ali, S.A.; Aadhar, S.; Shah, H.L.; Mishra, V. Projected Increase in Hydropower Production in India under Climate Change. *Sci. Rep.* **2018**, *8*, 12450. [CrossRef] [PubMed]
17. Ruin, I.; Creutin, J.-D.; Anquetin, S.; Lutoff, C. Human exposure to flash floods—Relation between flood parameters and human vulnerability during a storm of September 2002 in Southern France. *J. Hydrol.* **2008**, *361*, 199–213. [CrossRef]
18. Skilodimou, H.D.; Bathrellos, G.D.; Chousianitis, K.; Youssef, A.M.; Pradhan, B. Multi-hazard assessment modeling via multi-criteria analysis and GIS: A case study. *Environ. Earth Sci.* **2019**, *78*, 47. [CrossRef]
19. Moawad, B.M.; Abdel Aziz, A.O.; Mamtimin, B. Flash floods in the Sahara: A case study for the 28 January 2013 flood in Qena, Egypt. *Geomat. Nat. Hazards Risk* **2016**, *7*, 215–236. [CrossRef]
20. Kenyon, P. Climate connections: Algeria vs. the Sahara, NPR's climate connections series with National Geographic. 2007. Available online: <https://www.npr.org/templates/story/story.php?storyId=12903558> (accessed on 15 July 2019).
21. Irin. Preparing for floods in West Africa. 2013. Available online: <http://www.irinnews.org/news/2013/06/14> (accessed on 15 July 2019).
22. Youssef, A.M.; Hegab, M.A. Flood-Hazard Assessment Modeling Using Multi-Criteria Analysis and GIS: A Case Study: Ras Gharib Area, Egypt. In *Spatial Modeling in GIS and R for Earth and Environmental Sciences*, 1st ed.; Elsevier: Amsterdam, The Netherlands, 2019; p. 796.
23. Youssef, A.M.; Pradhan, B.; Sefry, S.A. Flash flood Susceptibility mapping in Jeddah city (Kingdom of Saudi Arabia) using bivariate and multivariate statistical models. *Env. Earth Sci.* **2016**, *75*. [CrossRef]
24. Youssef, A.M.; Sefry, S.A.; Pradhan, B.; Abu Al Fadail, E. Analysis on causes of flash flood in Jeddah city (Kingdom of Saudi Arabia) of 2009 and 2011 using multi-sensor remote sensing data and GIS. *Geomat. Nat. Haz. Risk* **2016**, *7*, 1018–1042. [CrossRef]
25. Sachin, D. Dam Break Analysis Using Mike11. Master Thesis, Department of Civil Engineering, National Institute of Technology, Rourkela, Odisha, India, May 2014; pp. 1–85.
26. Bezuayehu, T. People and Dams: Environmental and social-economic changes induced by a reservoir Fincha'a watershed, western Ethiopia. Ph.D. Thesis, Wageningen University, Wageningen, The Netherlands, June 2006; pp. 1–150.
27. Duressa, J.N. Dam Break Analysis and Inundation Mapping, Case Study of Fincha'a Dam in Horro Guduru Wollega Zone, Oromia Region, Ethiopia. *Sci. Res.* **2018**, *6*, 29. [CrossRef]

28. Xiong, Y. A Dam Break Analysis Using HEC-RAS. *J. Water Resour. Prot.* **2011**, *3*, 370–379. [[CrossRef](#)]
29. Abdulrahman, D.Z. Case Study of the Chaq-Chaq Dam Failure: Parameter Estimation and Evaluation of Dam Breach Prediction Models. *J. Eng. Res. Appl.* **2014**, *4*, 109–116.
30. Altinakar, M. *Modeling Tools for Dam Break Analysis*; National Center for computational Hydroscience and Engineering: Oxford, MS, USA, 2008.
31. Billa, L.; Shatttri, M.; Mahmud, A.R.; Ghazali, A.H. Comprehensive planning and the role of SDSS in flood disaster management in Malaysia. *Disaster Prev. Manag. Int. J.* **2006**, *15*, 233–240. [[CrossRef](#)]
32. Billa, L.; Mansor, S.; Mahmud, A. Pre-flood inundation mapping for flood early warning. *J. Flood Risk Manag.* **2011**, *4*, 318–327. [[CrossRef](#)]
33. Feng, C.-C.; Wang, Y.-C. GIScience research challenges for emergency management in Southeast Asia. *Nat. Hazards* **2011**, *59*, 597–616. [[CrossRef](#)]
34. Liu, Y.B.; De Smedt, F.; Smedt, F. Flood Modeling for Complex Terrain Using GIS and Remote Sensed Information. *Water Resour. Manag.* **2005**, *19*, 605–624. [[CrossRef](#)]
35. Takeuchi, K. ICHARM calls for an alliance for localism to manage the risk of water related disasters. In *Frontiers in flood research*; Tchiguirinskaia, I., Thein, K.N.N., Hubert, P., Eds.; IAHS Press: Paris, France, 2006; pp. 197–208.
36. The National Flood Risk Advisory Group (NFRAG). Flood risk management in Australia. *Aust. J. Emerg. Manag.* **2008**, *23*, 21–27.
37. Wang, Y.; Colby, J.D.; Mulcahy, K.A. An efficient method for mapping flood extent in a coastal floodplain using Landsat TM and DEM data. *Int. J. Remote. Sens.* **2002**, *23*, 3681–3696. [[CrossRef](#)]
38. Bates, P.D. Remote sensing and flood inundation modelling. *Hydrol. Process.* **2004**, *18*, 2593–2597. [[CrossRef](#)]
39. Merwade, V.; Cook, A.; Coonrod, J. GIS techniques for creating river terrain models for hydrodynamic modeling and flood inundation mapping. *Environ. Model. Softw.* **2008**, *23*, 1300–1311. [[CrossRef](#)]
40. Salimi, S.; Ghanbarpour, R.M.; Solaimani, K.; Ahmadi, M.Z. Flood plain mapping using hydraulic simulation model in GIS. *J. Appl. Sci.* **2008**, *8*, 660–665.
41. Khan, S.I.; Hong, Y.; Wang, J.; Yilmaz, K.K.; Gourley, J.J.; Adler, R.F.; Brakenridge, G.R.; Policelli, F.; Habib, S.; Irwin, D. Satellite remote sensing and hydrologic modeling for flood inundation mapping in Lake Victoria basin: Implications for hydrologic prediction in ungauged basins. *Geosci. Remote Sens. IEEE Trans.* **2011**, *49*, 85–95. [[CrossRef](#)]
42. Turner, A.B.; Colby, J.D.; Csontos, R.M.; Batten, M. Flood Modeling Using a Synthesis of Multi-Platform LiDAR Data. *Water* **2013**, *5*, 1533–1560. [[CrossRef](#)]
43. Nasab, A.R.; Norouzi, A.; Kim, S.; Habibi, H.; Nazari, B.; Seo, D.-J.; Lee, H.; Cosgrove, B.; Cui, Z. Toward high-resolution flash flood prediction in large urban areas—Analysis of sensitivity to spatiotemporal resolution of rainfall input and hydrologic modeling. *J. Hydrol.* **2015**, *531*, 370–388.
44. Köppen, W. Die Wärmezonen der Erde, nach der Dauer der heissen, gemässigten und kalten Zeit und nach der Wirkung der Wärme auf die organische Welt betrachtet. *Meteorol. Z.* **1884**, *20*, 215–226.
45. Peel, M.C.; Finlayson, B.L.; McMahon, T.A. Updated world map of the Köppen-Geiger climate classification. *Hydrol. Earth Syst. Sci.* **2007**, *11*, 1633–1644. [[CrossRef](#)]
46. AQUAVEO. *Watershed Modeling System WMS 10.0 Tutorials*; Aquaveo: Provo, UT, USA, 2016; Available online: <http://www.aquaveo.com/> (accessed on 15 June 2019).
47. HYFRAN Manual. Developed by INRS-Eau with Collaboration of Hydro-Quebec Hydraulic. 1998. Available online: <https://www.wrplc.com/books/HyfranPlus/hyfranplusgeneralinfo.html> (accessed on 28 February 2019).
48. Hershfield, D.M. Estimating the probable maximum precipitation. *J. Hydraul. Div.* **1961**, *87*, 99–106.
49. Hershfield, D.M. Method for Estimating Probable Maximum Precipitation. *J. Am. Waterworks Assoc.* **1965**, *57*, 965–972. [[CrossRef](#)]
50. ERDAS. *ERDAS Imagine 2014*; Hexagon Geospatial: Norcross, GA, USA, 2014.
51. ESRI. *ArcGIS for Desktop, Version 10.2*; Environmental Systems Research Institute: Redlands, CA, USA, 2013; Available online: <http://www.esri.com> (accessed on 5 February 2020).
52. US Army Corps of Engineers (USACE). *Hydrologic Modeling System HEC-HMS Technical Reference Manual*; Hydrologic Engineering Center: Davis, CA, USA, 2000.
53. UNDRO. *Mitigating Natural Disasters; Phenomena, Effects and Options*. United Nations Publication, UNDRO/MND/1990 Manual: Geneva, Switzerland, 1991.

54. Tingsanchali, T.; Karim, M.F. Flood hazard and risk analysis in the southwest region of Bangladesh. *Hydrol. Process.* **2005**, *19*, 2055–2069. [\[CrossRef\]](#)
55. Tingsanchali, T.; Karim, F. Flood-hazard assessment and risk-based zoning of a tropical flood plain: Case study of the Yom River, Thailand. *Hydrol. Sci. J.* **2010**, *55*, 145–161. [\[CrossRef\]](#)
56. Pradhan, B.; Youssef, A. A 100-year maximum flood susceptibility mapping using integrated hydrological and hydrodynamic models: Kelantan River Corridor, Malaysia. *J. Flood Risk Manag.* **2011**, *4*, 189–202. [\[CrossRef\]](#)
57. Biringer, B.; Danneels, J.J. Risk assessment methodology for protecting our critical physical infrastructures. In *Risk-Based Decisionmaking in Water Resources IX*; Haimes, Y.Y., Moser, D.A., Stakhiv, E.Z., Eds.; ASCE Publication: Santa Barbara, CA, USA, 2000; pp. 33–43.
58. Dutta, D.; Herath, S.; Musiake, K. A mathematical model for flood loss estimation. *J. Hydrol.* **2003**, *277*, 24–49. [\[CrossRef\]](#)
59. World Meteorological Organization. Manual for estimation of probable maximum precipitation (WMO No. 1045), 2009, Geneva, Switzerland. Available online: https://library.wmo.int/index.php?lvl=notice_display&id=1302#.XjVJt2gzZRY (accessed on 15 December 2015).
60. Luk, K.C.; Ball, J.E. *Application of GIS for Modelling of the Spatial Distribution of Rainfall*; Water Research Laboratory, University of New South Wales: Sydney, NSW, Australia, 1996. [\[CrossRef\]](#)
61. Chiles, J.P.; Delfiner, P. *Geostatistics Modelling Spatial Uncertainty*; Wiley Series in Probability and Statistics; John Wiley & Sons Inc.: Hoboken, NJ, USA, 2012. [\[CrossRef\]](#)
62. Laity, J.E. Deserts and desert environments. Wiley-Blackwell: Oxford, UK, 2008; p. 360.
63. Pietersen, J.; Gericke, O.; Smithers, J.; Woyessa, Y. Review of current methods for estimating areal reduction factors applied to South African design point rainfall and preliminary identification of new methods: Technical paper. *J. South Afr. Inst. Civ. Eng.* **2015**, *57*, 16–30. [\[CrossRef\]](#)
64. Alexander, W.J.R. *Flood Hydrology for Southern Africa*; SANCOLD: Pretoria, South Africa, 1990.
65. Alexander, W.J.R. *Flood Risk Reduction Measures: Incorporating Flood Hydrology for Southern Africa*; Department of Civil and Biosystems Engineering, University of Pretoria: Pretoria, South Africa, 2001.
66. Engineering specification rules for flood prevention in Ar Riyadh city (2017). Manual of water drainage networks design, real reduction factor for basin area; p. 44, S14026-0100D-RPT-PM-07-REV 2. Available online: <https://sd.alriyadh.gov.sa/> (accessed on 10 May 2017).
67. Soil Conservation Services (SCS). *National Engineering Handbook, Section 4: Hydrology*; US Department of Agriculture, Soil Conservation Service, Engineering Division: Washington, DC, USA, 1985.



© 2020 by the authors. Licensee MDPI, Basel, Switzerland. This article is an open access article distributed under the terms and conditions of the Creative Commons Attribution (CC BY) license (<http://creativecommons.org/licenses/by/4.0/>).